proceedings

MDPI

Proceedings

Hirshfeld Surface Analysis and Energy Framework for Crystals of Quinazoline Methylidene Bridged Compounds †

Akmaljon Tojiboev [1,*], Sherzod Zhurakulov [2,3], Ulli Englert [4], Ruimin Wang [4], Irmgard Kalf [4], Valentina Vinogradova [2], Kambarali Turgunov [2,5] and Bakhodir Tashkhodjaev [2]

1 Laboratory of Multiphase Systems Thermophysics, Arifov Institute of Ion-Plasma and Laser Technologies, Uzbekistan Academy of Sciences, Yuli St. 33, Tashkent 100125, Uzbekistan
2 S. Yu. Yunusov Institute of Chemistry of Plant Substances, Academy of Sciences of Uzbekistan, Mirzo Ulugbek Str. 77, Tashkent 100170, Uzbekistan; j.sherzod.78@mail.ru (S.Z.); cnc@icps.org.uz(V.V.); qambarr@yahoo.com (K.T.); tashkhodjaev@rambler.ru (B.T.)
3 Department of Organic Chemistry, Faculty of Chemistry, National University of Uzbekistan named after Mirzo Ulugbek, University Str. 4 Olmazor District, Tashkent 100174, Uzbekistan
4 Institute of Inorganic Chemistry, RWTH Aachen University, Landoltweg 1, 52056 Aachen, Germany; ullrich.englert@ac.rwth-aachen.de (U.E.); ruimin.wang@ac.rwth-aachen.de (R.W.); irmgard.kalf@ac.rwth-aachen.de (I.K.)
5 Department of Natural-Mathematical Sciences, Turin Polytechnic University in Tashkent, Kichik Khalka Yuli Str. 17, Tashkent 100095, Uzbekistan
* Correspondence: a_tojiboev@yahoo.com
† Presented at the 2nd International Electronic Conference on Crystals, 10–20 November 2020; Available online: https://iocc_2020.sciforum.net/.

Published: 18 December 2020

Abstract: The crystal structures of 4-(3,4-dimethoxyphenylethylamino)-methylidene-2,3,4,10-tetrahydro-1H-pyrido[2,1-b]-quinazolin-10-one (**1**) and 4-(3,4-methylene-dioxyphenylethylamino)-methylidene-2,3,4,10-tetrahydro-1H-pyrido[2,1-b]-quina-zolin-10-one hydrochloride (**2**) were studied by single crystal X-ray diffraction. Their molecular and crystal structures are described in the context of intra- and inter-molecular interactions and of stereoisomerism. The crystallographic study established mixed *E*, *Z* configuration about the C4=C12 bond for (**1**) and *E* configuration about the C4=C12 bond for (**2**). For molecular crystals, Hirshfeld surface analyses may provide insight into intermolecular interactions, and energy framework analyses allow one to quantify different contributions to the overall energy. These analyses were performed to pinpoint intermolecular interactions in (**1**) and (**2**). According to our results, the molecules are associated with intra- and intermolecular hydrogen bonds, C-H···π and π-stacking interactions. The three-dimensional Hirshfeld surface analyses and two-dimensional fingerprint plots revealed that the structures are dominated by H···H, H···C/C···H and H···O/O···H contacts. The intermolecular energy analysis confirmed a significant contribution of dispersion to the stabilization of molecular packings in (**1**) and (**2**).

Keywords: crystal structure; quinazoline; intermolecular interaction energy

1. Introduction

Quinazoline alkaloids are heterocycles containing tricyclic rings and represent an interesting group among alkaloids found in plants of the genus *Peganum, Adhatoda, Galega, Galium, Nitraria*, etc. [1,2]. Alkaloids with biological activity and use in medical practice have been found in this series. Among them, deoxypeganine and deoxyvazicinone isolated from the plant Peganum harmala are

particularly interesting. Deoxypeganine is an anticholinesterase drug in the form of the deoxypeganine hydrochloride [3,4]. Deoxyvazicinone shows antimicrobial and anti-inflammatory activity [5,6]. The alkaloid makinazolinone was first isolated from the plant Mackilaya subulata Philipson [7]. In order to identify factors relevant for the reactivity of 4-(formyl)-2,3,4,10-tetratahydro-1H-pyrido[2,1-b]-quinazoline-10-one (**I**) towards nucleophilic substitution, we carried out the amination reaction 4-(formyl)-2,3,4,10-tetratahydro-1H-pyrido[2,1-b]-quinazoline-10-one (**I**) c 3,4-dimethoxyphenylethylamine (**II**) and 3,4-methylenedioxyphenylethylamine (**III**) according to a published method [8–12] and obtained the derivatives (**1**) and (**2**). These studies continue our research in this direction [13]. A reaction scheme for the synthesis of the title compounds is illustrated in Scheme 1. In this contribution, we describe the molecular and crystal structures of the target compounds and perform a Hirshfeld surface analysis to visualize intermolecular interactions.

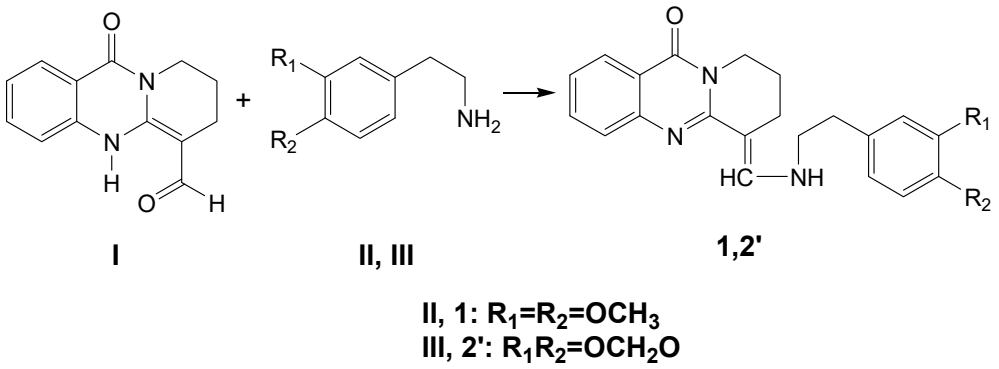

Scheme 1. Reaction scheme.

2. Materials and Methods

2.1. General Experiment and Synthesis

A detailed report on the synthesis of (**1**), (**2**) and its characterization by IR, ^{1}H NMR is available in [14–16]. Synthesis of 4-(3,4-Methylenedioxyphenylethylamino)-methylidene-2,3,4,10-tetrahydro-1H-pyrido[2,1-b]-quinazolin-10-one hydrochloride (**2**): 4-(3,4-methylenedioxyphenylethylamino)-methylidene-2,3,4,10-tetrahydro-1H-pyrido[2,1-b]-quinazolin-10-one (**2'**) was dissolved in acetone and acidified with concentrated HCI to pH 5-6. The precipitated hydrochloride was separated by filtration and recrystallized from methanol. Crystals suitable for X-ray diffraction were obtained from a solution in methanol by slow evaporation of the solvent at room temperature.

2.2. Crystallographic Details

Crystal diffraction data were collected: for (**1**) on a Bruker D8 diffractometer equipped with an APEX CCD detector and multilayer optics microfocus tube with MoKα radiation and for (**2**) on the EH1 Kappa diffractometer equipped with a Dectris CdTe area detector using synchrotron radiation at beamline P24, DESY, Hamburg. The crystals of (**1**) were extremely small; because of this, it was used for synchrotron radiation. Absorption correction was not applied for (**1**). Crystal structures of (**1**) and (**2**) were solved by direct methods with the program SHELXS [17] and refined by full-matrix least-squares on F^2 with the SHELXL [18] package.

In the crystal structure (**1**), H atoms attached to C were positioned geometrically and treated as riding on their parent atoms, with C-H = 0.95 (aromatic), 0.98 (methyl), 0.99 (methylene) Å and were refined with U_{iso}(H) = 1.5U_{eq}(C) for methyl H atoms and 1.2U_{eq}(C) otherwise. The H atom in the enamine group was refined with a distance restraint (target distance N-H = 0.95 Å) and with U_{iso}(H) = 1.2U_{eq}(N). The residual density is high (0.85 e Å^{-3}) due to the extensive disorder.

In the crystal structure of (**2**), H atoms attached to C were positioned geometrically and treated as riding on their parent atoms, with C-H = 0.95 (aromatic), 0.99 (methylene) Å and were refined with

1.2U_{eq}(C) otherwise. The H atom bonded to nitrogen was constrained with a distance 0.88 A° and with U_{iso}(H) = 1.2U_{eq}(N).

Details of the crystallographic data collection, structural determination and refinement for (**1**) and (**2**) are summarized in Table S1 (see Supplementary Materials). The full dataset is available in form of CIF files, deposited with the CCDC (2039173, 2039174), and may be obtained free of charge via https://www.ccdc.cam.ac.uk/structures.

2.3. Hirshfeld Surface Calculations

The Hirshfeld surface (HS) is the area around a molecule in crystal space which separates two regions, that of the inner reference molecule from the outer neighboring molecules. The separation of space by the HS allows the analysis of intermolecular interactions of fingerprints in a crystalline medium [19,20]. HS analysis can be employed to visualize and quantify various non-covalent interactions that stabilize the crystal packing. HS can be mapped with different properties, namely, d_{norm}, electrostatic potential, shape index and curvature. The d_{norm} property is a symmetric function of distances to the surface between nuclei inside and outside the Hirshfeld surface (d_i and d_e, respectively), relative to their respective van der Waals radii. The regions with red and blue color on the d_{norm} represent the shorter and longer inter contacts while the white color indicates the contacts around the van der Waals radii. Two-dimensional fingerprint plots provide relevant information of intermolecular contacts in the crystal. HS analysis has become a very useful tool for explaining the nature of intermolecular interactions that affect the packing of molecules in crystals [21]. Hirshfeld surfaces analyses are widely used to study the phenomena of polymorphism [22,23], co-crystallization [24], the inclusion of small molecules in the cavities of macromolecules [25,26], and the search for correlations between the strength of interactions and the melting point [27].

The HS analyses and their associated 2D fingerprint plots (full and decomposed) [28] were carried out employing the CrystalExplorer 17.5 program [29]. The d_{norm} surface was mapped with the color scale in the range −0.050 au (red) to 0.600 au (blue). The 2D fingerprint plots (d_i vs. d_e) were displayed using the expanded 0.6–2.8 Å range.

3. Results and Discussion

3.1. Structural Description

The compounds (1) and (2) crystallize in the monoclinic system in space group $P2_1/c$. Displacement ellipsoid plots and numbering schemes for both molecules are provided in Figure 1.

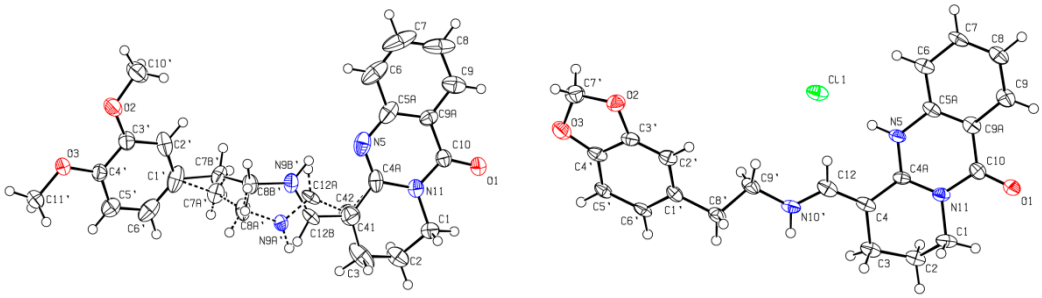

(**a**) (**b**)

Figure 1. Displacement ellipsoid plot [30] of the asymmetric unit of: (**a**) 4-(3,4-dimethoxyphenylethylamino)-methylidene-2,3,4,10-tetrahydro-1*H*-pyrido[2,1-b]-quinazolin-10-one (**1**); (**b**) of 4-(3,4-methylenedioxyphenylethylamino)-methylidene-2,3,4,10-tetrahydro-1*H*-pyrido[2,1-b]-quinazolin-10-one hydrochloride (**2**) and atom-labeling scheme. Ellipsoids are drawn at 50% probability; H atoms are shown as spheres of arbitrary radius.

For the structure of (**1**), X-ray diffraction revealed that the binding enamine group is disordered, leading to the formation of *E* and *Z* isomers about the C4=C12 double bond. In case of the *E* configuration, an O···H-N intermolecular hydrogen bond links the N atom of the enamine group to the keto group of the quinazoline moiety and gives rise to a $C_1^1(8)$ chain motif connecting adjacent molecules to zigzag like chains propagating along the *b*-axis (Figure 2a). In the case of the *Z* configuration, an N9B′-H9B′···N5 intramolecular hydrogen bond (2.812(8) Å) is formed, which generates an $S_1^1(6)$ ring motif (Figure 2b). In both cases, an additional C6-H6···O2 hydrogen bond leads to a two-dimensional network parallel to (102) plane (Figure 2a,b and Figure S1). The hydrogen-bond geometry for (**1**) is listed in Table S2.

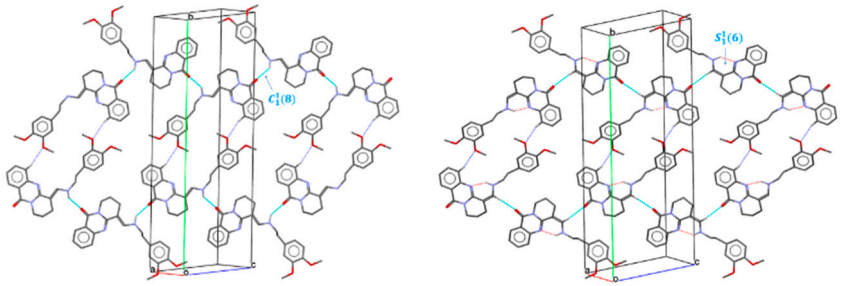

(**a**) (**b**)

Figure 2. Packing for the alternative configurations of (**1**) along the *b*-axis, showing interactions in the layers. C-H···O hydrogen bonds as dark blue dashed lines; (**a**) O···H-N intermolecular hydrogen bonds are represented as light-blue dashed lines, which generate a $C_1^1(8)$ ring motif forming *E* configuration; (**b**) N-H···N intramolecular hydrogen bonds as red dashed lines, which generate an $S_1^1(6)$ ring motif forming *Z* configuration. H atoms not involved in hydrogen bonds have been omitted for clarity.

Figure 3a shows the interaction between adjacent molecules along the crystallographic *a*-axis. *Cg*4 denotes the centroid of the 3,4-dimethoxyphenylethylamino ring (C1′-C6′). In the *Z*-configuration of (**1**), both contacts C7B′-H7BB···*Cg*4 and C11′-H11B···*Cg*4 participate in the interaction between adjacent molecules, whereas in the case of the *E*-configuration, only the latter contact contributes to C-H···π interactions.

Structure (**2**) consists of Cl^- counter anions and the organic cations. The latter are composed of tricyclic quinazoline and 3,4-methylenedioxyphenylethylamino units linked by an enamine group (Figure 1b). The crystallographic study of structure (**2**) revealed the *E* configuration about the C4=C12 double bond, similar to one of the alternative configurations in structure (**1**) (Figure 1b). N5-H5 Cl1 (3.088(5)Å) and N10′-10′ Cl1(3.187(6)Å) intermolecular hydrogen bonds links the Cl^- anion to N atoms in the enamine group and the pyrimidine ring and give rise to a centrosymmetric dimer (Figure S2 and Table S3) with $D_1^1(2)$, $R_4^2(16)$ graph motif. Additional short ring interactions *Cg*1-*Cg*5 (3.758(5)Å), *Cg*2-*Cg*4 (3.426(4)Å) and *Cg*4-*Cg*5 (3.662(4)Å) lead to formation of a three dimensional supramolecular network (*Cg*1(O1/C3′/C4′/O3/C7), *Cg*2(N5/C4A/N11/C10/C9A/C5A), *Cg*4(C1′-C6′) and *Cg*5(C5A/C6-C9/C9A) (Figure 3b).

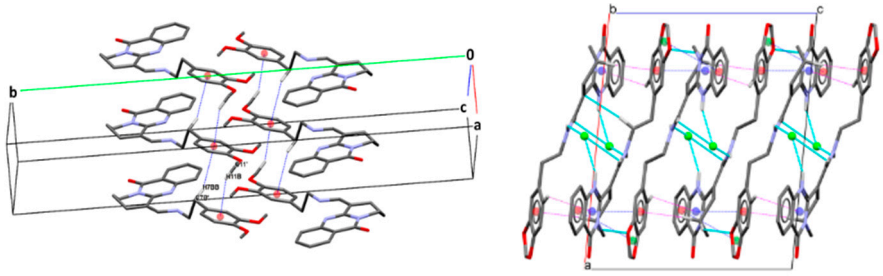

(**a**) (**b**)

Figure 3. (**a**) C-H···π interactions between layers in (1); H atoms not involved in the interactions have been omitted. (**b**) Packing diagram viewed along the b-axis with the interactions C-H···O, C-H···Cl, N-H···Cl shown as blue dashed lines, C-H···π (ring) and π—stacking interactions shown as magenta and dark blue dashed lines. Ring centroids are as spheres: *Cg*1-green; *Cg*2-blue; *Cg*4 and *Cg*5-red. H atoms not involved in hydrogen bonds have been omitted.

3.2. Hirshfeld Surface Analysis

The intermolecular interactions in (**1**) and (**2**) have been further investigated and visualized by HS analyses performed with CrystalExplorer17.5 [29]. d_{norm} mapped on the HS (Figure 4a,b) shows short intermolecular contacts as red spots. They correspond to C-H···O contacts in (**1**) (Figure 5a) and C-H···O and N-H···Cl hydrogen bonds in (**2**) (Figure 5b).

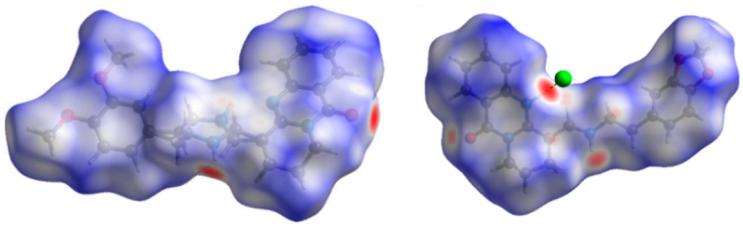

(**a**) (**b**)

Figure 4. View of the three-dimensional Hirshfeld surface: (**a**) of (**1**) plotted over d_{norm} in the range –0.5234 to 1.2437 a.u.; (**b**) of (**2**) plotted over d_{norm} in the range −0.5144 to 1.2154.

The overall fingerprint plot for (**1**) and (**2**) is shown in Figures 5a,f, respectively, and those decomposed into H···H, H···C/C···H, H···O/O···H, H···N/N···H and Cl···H/H···Cl contacts are illustrated in Figure 5(b–e,g–j) together with their relative contributions to the Hirshfeld surface.

The most prominent type of contacts in (**1**) structure corresponds to H···H contacts; they contribute 56.5% to the overall surface contacts (Figure 5b). The presence of C—H···π interactions gives rise to a pair of characteristic wings in the fingerprint plot decomposed into C···H/H···C contacts (Figure 5c) contributing 21.4% to the HS. Short O···H/H···O contacts (Figure 5d) contribute 14.5% to the HS and form a pair of spikes. N···H/H···N contacts, contributing 2.6% to the overall surface, are depicted in Figure 5e as widely scattered wings.

For the structure (**2**), the fingerprint profile is dominated by H···H (44.4%) surface contacts (Figure 5g). C···H/H···C interactions contribute 17.0% of the total HS (Figure 5h) as pair wings. The pair of sharp spikes (Figure 5i) represents the H···O/O···H contacts with a contribution of 16.8%; they are due to intermolecular C-H···O hydrogen bonding. The fingerprint plot for Cl...H/H...Cl contacts (10.9% contribution) in Figure 5j has a pair of spikes indicating C-H···Cl contacts.

The contributions of other contacts to the Hirshfeld surface are negligible for both structures; they amount to H···N/N···H (2.6%), C···C (2.3%), C···N/N···C (1.8%), O···C/C···O (0.5%), N···N (0.3%) for (**1**) and to H···N/N···H (2.4%), C···N/N···C (1.7%), O···C/C···O (1.1%), O···O (0.4%), N···N (0.1%) for (**2**).

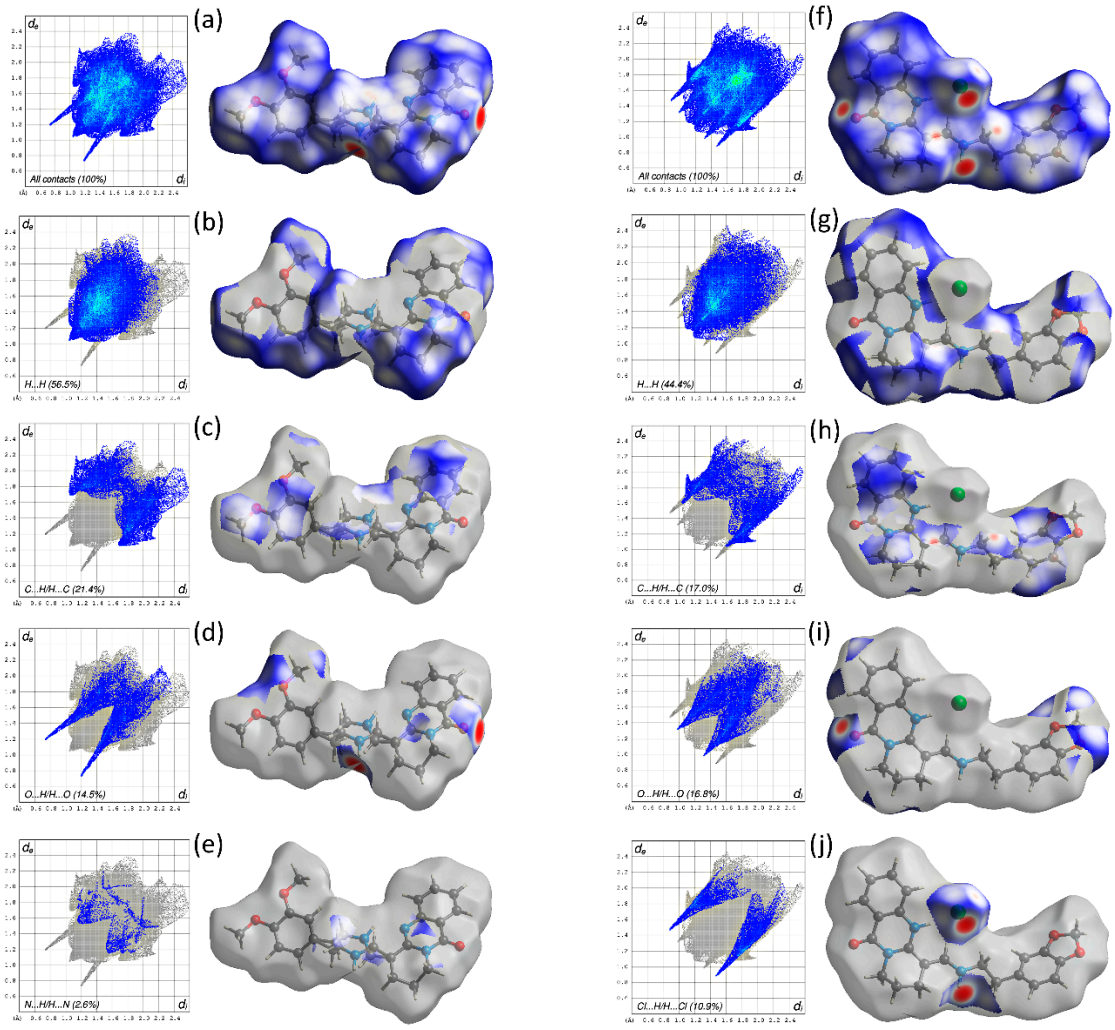

Figure 5. Two-dimensional fingerprint plots for all intermolecular contacts in (**1**) (**a**) and (**2**) (**f**). Contributions of individual interactions: H···H for (**1**) (**b**) and (**2**) (**g**); C···H/H···C for (**1**) (**c**) and (**2**) (**h**); O···H/H···O for (**1**) (**d**) and (**2**) (**i**); N···H/H···C for (**1**) (**e**) and Cl···H/H···Cl for (**2**) (**j**). The outline of the full fingerprint plot is shown in grey. Surfaces to the right highlight the relevant d_{norm} surface patches associated with the specific contacts. The percentage of contribution is specified for each contact.

3.3. Interaction Energies

Interaction energies in (**1**) and (**2**) were calculated using CE-B3LYP/6-31G(d,p) quantum level of theory, as available in CrystalExplorer. The total intermolecular interaction energy (E_{tot}) is the sum of four energy terms: electrostatic (E_{ele}), polarization (E_{pol}), dispersion (E_{disp}) and exchange-repulsion (E_{rep}) with scale factors of 1.057, 0.740, 0.871 and 0.618, respectively [31]. The relative strengths in interaction energies in individual directions are represented by cylinder-shaped energy frameworks (Figures 6). Insignificant contacts weaker than a threshold energy of 10 kcal/mol have been omitted from the original figure for clarity. Dispersion forces play the dominant role in (**1**) and (**2**) (Figure 6).

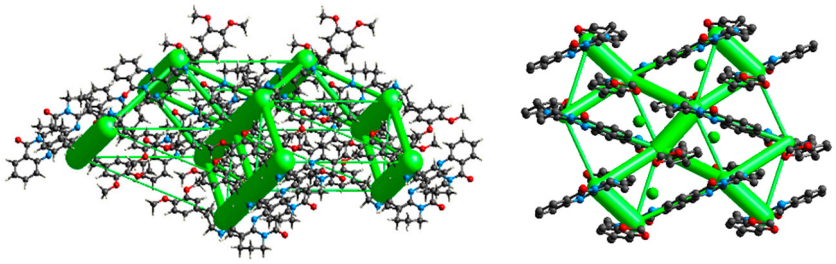

Figure 6. Energy-framework diagrams for E_{dis} for a cluster of molecules in (**1**) and (**2**). The cylindrical radius is proportional to the relative strength of the corresponding energy and was adjusted to the scale factor of 80 kJ mol^{-1} with a cut-off value of 10 kJ mol^{-1}.

4. Conclusions

A detailed structural analysis of 4-(3,4-dimethoxyphenylethylamino)-methylidene-2,3,4,10-tetrahydro-1H-pyrido[2,1-b]-quinazolin-10-one revealed disorder of the enamine group, leading to the concomitant presence of *E* and *Z* isomers in the crystal. In the *E* isomer, an intramolecular N-H···O hydrogen bond results in the formation of a *C*(8) ring motif. In the *Z* isomer, an intramolecular N-H···N hydrogen bond results in the formation of an *S*(6) pattern. The large number of H···H, H···C/C···H and H···O/O···H contacts revealed by a HS analysis indicate that van der Waals interactions and hydrogen bonding mostly contribute to crystal packing. Initial results on energy frameworks suggest that dispersion forces are relevant to the topology of the overall interaction energies in these crystals of quinazoline derivatives.

Supplementary Materials: The following are available online at www.mdpi.com/xxx/s1, **Figure S1**: Layers are propagating parallel to (102) plane. H atoms not involved in interactions have been omitted for clarity; **Figure S2**: A partial packing diagram of the crystal of (**2**) with intramolecular C-H···O, C-H···N and intermolecular C-H···O, C-H···Cl, N-H···Cl hydrogen bonds shown, respectively, by red and blue dashed lines. H atoms not involved in hydrogen bonds have been omitted for clarity; **Table S1**: Crystal data and structure refinement parameters for (**1**) and (**2**); **Table S2**: Hydrogen-bond geometry (Å,º) for (**1**). *Cg*4 is the centroids of ring (C1′-C6′); **Table S3**: Hydrogen-bond geometry (Å,º) for (**2**). *Cg*2 and *Cg*4 are the centroids of ring (N5/C4A/N11/C10/C9A/C5A) and (C1′-C6′), respectively.

Author Contributions: A.T., S.Z., U.E. and K.T. conceived and designed the experiments, conceptualized the work, and prepared the manuscript for publication; U.E. conducted the X-ray analysis, reviewed, and edited the manuscript; U.E., R.W., B.T. and K.T. validated and formal analyzed; I.K. crystallization experiments; S.Z. and V.V. provided chemical synthesis; U.E. reviewed, and edited the manuscript. All authors have read and agreed to the published version of the manuscript.

Funding: This work was supported by the Istedod Foundation of the Republic of Uzbekistan.

Acknowledgments: We thank Carsten Paulmann for help with the synchrotron data collections and we are grateful to DESY for travel support.

Conflicts of Interest: The authors declare no conflict of interest.

References

1. Shoji, E. Quinazoline Alkaloids and Related Chemistry. *Heterocycl. Chem.* **2006**, *6*, 113–156.
2. Shakhidoyatov, K.M.; Elmuradov, B.Z. Tricyclic Quinazoline Alkaloids: Isolation, Synthesis, Chemical Modification, and Biological Activity. *Chem. Nat Compd.* **2014**, *50*, 781–800.
3. Mashkovskiy, M.D. *Medicines*; Medicine: Moscow, Russian, 1998. (In Russian)
4. Shakhidoyatov, K.M. *Khinazolony-4. Ikh Biologicheskaya Aktivnost*; FAN: Tashkent, Uzbekistan, 1988.
5. Al-Shamma, A.; Drake, S.; Flynn, D.L.; Mitscher, L.A.; Park, Y.H.; Rao, G.S.; Simpson, A.; Swayze, J.K.; Veysoglu, T.; Wu, S.T. Antimicrobial agents from higher plants. Antimicrobial agents from Peganum harmala seeds. *J. Nat. Prod.* **1981**, *44*, 745–747.

6. Tulyaganov, N. Pharmacological investigations of alkaloids Peganum harmala L. quinazoline and quinazolone structure and their derivatives. *Pharma. Nat. Compd.* **1979**, 71–80. (In Russian)
7. Fitzgerald, J.S.; Johns, S.R.; Lamberton, J.A.; Redcliffe, A.H. 6,7,8,9-Tetrahydropyridoquinazolines, a new class of alkaloids from Mackinlaya species (Araliaceae). *Aust. J. Chem.* **1966**, *19*, 151–159.
8. Elmuradov, B.Z.; Shakhidoyatov, K.M. Transformation of natural compounds. VII. Synthesis of α-piperazinyl methylidene deoxyvasicinones. *Chem. Nat. Compd.* **1998**, *34*, 298–299.
9. Elmuradov, B.Z., Chemical Modifications of α-oxy-, -chloro-, -hydroselenylmethylidene-2,3-trimethylene-3,4-dihydroquinazolin-4-ones. Ph.D. Thesis, National University of Uzbekistan, Tashkent, Uzbekistan, 2003.
10. Elmuradov, B.; Shakhidoyatov, K.M. Interaction of α-hydroxymethylidene-2,3-trimethylene-3,4-dihydroquinazolin-4-one with amines. *Chem. Chem. Technol.* **2008**, *3*, 27–31.
11. Turdibayev, Z.E.; Elmuradov, B.Z.; Khakimov, M.M.; Shakhidoyatov, K.M.; Formylation of deoxyvasicinone by alkylformates: Synthesis and reaction of α-hydroxymethylidenedeoxyvasicinone with isomeric aminophenols and aminobenzoic acids. *Chem. Nat. Compd.* **2011**, *47*, 600–603.
12. Nasrullaev, A.O.; Turdibayev, Z.E.; Elmuradov, B.Z.; Yili, A.; Aisa, H.A.; Shakhidoyatov, K.M. Chemical transformat ions of mackinazolinone and its derivatives. *Chem. Nat. Compd.* **2012**, *48*, 638–642.
13. Tojiboev, A.; Zhurakulov, S.; Vinogradova, V.; Englert, U.; Wang, R. Stereochemistry of the methylidene-bridged quinazoline-isoquinoline alkaloid 3-{[6,7-dimethoxy-1-(4-nitrophenyl) -1,2,3,4-tetrahydroisoquinolin-2-yl]-methylidene}-1,2,3,9-tetrahydropyrrolo[2,1-b]-quinazolin-9-one methanol monosolvate. *Acta Cryst. E* **2020**, *76*, 914–919.
14. Zhurakulov, S.N.; Vinogradova, V.I. Reaksiya 3-gidroksimetiliden-1,2,3,9- tetragidropirrolo[2,1-b]-hinazolin-9-ona i 4-(formil)-1,2,3,4,10-pentagidropirido[2,1-b]-hinazolin-10-ona s benzilaminom i psevdoefedrinom. *Uzb. Chem. J.* **2015**, *5*, 25–29.
15. Zhurakulov, Sh. N.; Vinogradova, V.I. 3-Hydroxymethylidene-1,2,3,9-tetrahydropyrrolo[2,1-b]-quinazolin-9-one and 4-(formyl)-1,2,3,4,10-pentahydropyrido[2,1-b]-quinazolin-10-one–new sintons for obtaining of 3,4-dihydroisoquinolines. *Int. J. Chem. Phys. Sci.* **2016**, *5*, 1–7.
16. Zhurakulov, Sh. N., Levkovich, M.G.; Vinogradova, V.I. Reactions of 3,4-Dimethoxyphenylethylaminomethylidene Derivatives Triand Tetramethylene-4-Quinazolones and Formaldehyde. *Chem. Sustain. Dev.* **2017**, *25*, 265–269.
17. Sheldrick, G.M. A short history of SHELX. *Acta Cryst. Sect. A* **2008**, *64*, 112–122.
18. Sheldrick, G.M. Crystal structure refinement with SHELXL. *Acta Cryst. C* **2015**, *71*, 3–8.
19. McKinnon, J.J.; Jayatilaka, D.; Spackman, M.A. Towards quantitative analysis of intermolecular interactions with Hirshfeld surfaces. *Chem. Commun.* **2007**, 3814–3816.
20. Spackman, M.A.; Jayatilaka, D. Hirshfeld surface analysis. *CrystEngComm* **2009**, *11*, 19–32.
21. Mitchell, A.S. Novel tools for visualizing and exploring intermolecular interactions in molecular crystals. *Acta Cryst. B* **2004**, *60*, 627–668.
22. Munshi, P.; Skelton, B.W.; McKinnon, J.J.; Spackman, M.A. Polymorphism in 3-methyl-4-methoxy-4′-nitrostilbene, a highly active NLO material. *CrystEngComm* **2008**, *10*, 197–206.
23. Lemmerer, A.; Bernstein, J.; Spackman, M.A. Supramolecular polymorphism of the 1:1 molecular salt (adamantane-1-carboxylate-3,5,7-tricarboxylic acid) (hexamethylenetetraminium). A "failed" crystal engineering attempt. *Chem. Commun.* **2012**, *48*, 1883–1885.
24. Luo, Y.H.; Sun, B.W. Co-crystallization of pyridine-2-carboxamide with a series of alkyl dicarboxylic acids with different carbon chain: Crystal structure, spectroscopy and Hirshfeld analysis. *Spectrochim. Acta A* **2014**, *120*, 228–236.
25. Nemkevich, A.; Spackman, M.A.; Corry, B. Simulations of Guest Transport in Clathrates of Dianins Compound andHydroquinone. *Chem. Eur. J.* **2013**, *19*, 2676–2684.
26. Lee, J.J.; Sobolev, A.N.; Turner, M.J.; Fuller, R.O.; Iversen, B.B.; Koutsantonis, G.A.; Spackman, M.A. Molecular Imprisonment: Host Response to Guest Location, Orientation, and Dynamics in Clathrates of Dianin's Compound. *Cryst. Growth Des.* **2014**, *14*, 1296–1306.
27. Grabowsky, S.; Dean, P.M.; Skelton, B.W.; Sobolev, A.N.; Spackman, M.A.; White, A.H. Crystal packing in the 2-R,4-oxo-[1,3-a/b]-naphtho dioxanes—Hirshfeldsurface analysis and melting point correlation. *CrystEngComm* **2012**, *14*, 1083–1093.
28. Spackman, M.A.; McKinnon, J.J. Fingerprinting intermolecular interactions in molecular crystals. *CrystEngComm* **2002**, *4*, 378–392.

29. Turner, M.J.; McKinnon, J.J.; Wolff, S.K.; Grimwood, D.J.; Spackman, P.R.; Jayatilaka, D.; Spackman, M.A. *Crystal Explorer 17*; University of Western Australia: Pert, Australia, 2017.
30. Spek, A.L. Checkcif validation ALERTS: What they mean and how to respond *Acta Cryst. E* **2020**, *76*, 1–11.
31. Mackenzie, C.F.; Spackman, P.R.; Jayatilaka, D.; Spackman, M.A. CrystalExplorer model energies and energy frameworks: Extension to metal coordination compounds, organic salts, solvates and open-shell systems. *IUCrJ* **2017**, *4*, 575–587.